

Preparation of Zinc Oxide Nanomaterial and Research and Development of Antibacterial Property

Jia Huang

School of Environment Design, Hunan International Economics University, Changsha 410205, China

Corresponding Author Email: huangjia1204@163.com



<https://doi.org/10.18280/acsm.450507>

ABSTRACT

Received: 13 July 2021

Accepted: 20 August 2021

Keywords:

zinc oxide (ZnO) nanomaterial, preparation, antibacterial property, children's furniture

Children using environmentally unfriendly furniture are more likely to suffer from allergic rhinitis, respiratory infections, and leukemia. The green design of children's furniture must consider anti-formaldehyde, deodorant, antibacterial, and antiviral factors. This paper prepares a zinc oxide (ZnO) nanomaterial for children's furniture, and researches and develops the antibacterial property of the nanomaterial. The main contents include the synthesis method and preparation process, material morphology and structure characterization, and antibacterial performance testing. The practical substrate modification of the material was realized by pre-depositing polydopamine particles. In this way, the ZnO nanomaterial could apply to a wider range of children's furniture, become more durable, and realize efficient multi-mechanism synergistic sterilization. Experimental results show that the prepared material has a good antibacterial property.

1. INTRODUCTION

Green living is an increasingly popular concept. Safe and high-quality green furniture, especially children's wooden furniture, has become the core demand of consumers [1-6]. Children using environmentally unfriendly furniture are more likely to suffer from allergic rhinitis, respiratory infections, and leukemia [7-12]. The green design of children's furniture must consider all the factors that might endanger their health, such as anti-formaldehyde, deodorant, antibacterial, and antiviral factors [13-17]. Zinc oxide (ZnO) nanomaterial provides a special paint for children's furniture, enabling functions like sterilization, health care, formaldehyde removal, stain resistance, and anti-aging.

Hermida-Montero et al. [18] reported the in vitro antifungal activity of ZnO nanoparticles against three symbiotic fungi of ragweed beetle, and studied the coating and particle size of two types of ZnO nanoparticles on antifungal activity. Experiments show that, although nanoparticle size is a key parameter, the coating of ZnO nanoparticles is the leading contributor to antifungal performance. La et al. [19] prepared ZnO nanoparticles by hydrothermal method, and characterized them by scanning electron microscopy (SEM) and X-ray diffraction (XRD). The prepared ZnO nanoparticles showed good antibacterial properties against several bacteria, including *Staphylococcus aureus*, *Escherichia coli* and *Bacillus subtilis*. Li et al. [20] presented a simple method for preparing superhydrophobic coatings based on acrylic resins: ZnO nanoparticles are modified with silane to obtain hydrophobic ZnO, which is uniformly blended with acrylic resin, and then the mixture is sprayed onto the aluminum plate, forming a cured coating. Experimental results verify that the antibacterial performance of the ZnO nanoparticles/acrylic resin superhydrophobic coating is much better than pure acrylic resin coating.

The hydrophobicity and color stability are important

features of wood. When wood is used as a raw material for outdoor products, these features are easy to change, thereby shortening the service life of the wood. Tuong et al. [21] adopted a two-step simple spraying method to apply ZnO coating to benzoin wood, aiming to improve hydrophobicity and color stability of the wood, the hydrophobicity and firmness of the coating, and the color stability of uncoated wood samples. Then, they evaluated the coated wood samples. Pang et al. [22] prepared a ZnO/TiO₂ nano-array coating through hydrothermal synthesis and low-temperature liquid phase method. In vitro antibacterial experiments show that the bacterium has a maximum inhibitory rate of 99% against *Staphylococcus aureus* and 90% against *Escherichia coli*.

This paper focuses on the preparation of a ZnO nanomaterial for children's furniture, and the research and development of antibacterial property. The main contents are as follows: After summing up the strengths and defects of ZnO nanomaterial, Section 2 specifies the principle and flow of preparing Zinc nano-array for high-temperature hard materials like metal handles, and wooden plates in children's furniture, respectively, and analyzes the antibacterial mechanism and antibacterial performance of the zinc nano-array. Section 3 improves the enrichment of ZnO nanocrystals on cellulose by pre-depositing polydopamine particles, and explains the process of antibacterial performance determination and thermogravimetric analysis. Section 4 carries out comparative experiments to demonstrate the good antibacterial property of the prepared modified material.

2. PREPARATION AND ANTIBACTERIAL PROPERTY OF ZNO NANO-ARRAY

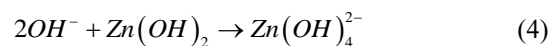
2.1 Preparation and characterization

Whether the environment is bright or dark, the ZnO, as an active oxide produced by catalytic reaction, always has an

excellent antibacterial effect. However, the chemical antibacterial mechanism depends on the release of active oxygen, and generally faces problems like the slow active effect, the short life of active oxides, the potential microbial mutation, and the development of drug resistance. To solve these problems, it is particularly important to find a new antibacterial method. Inspired by the physical sterilization of bionic nanostructures, some scholars have constructed ZnO nano-arrays, which not only pierce through bacteria, but also achieve significant photocatalytic self-cleaning and functional regeneration.

Taking nano-ZnO array as the object, this paper describes the synthesis method and the preparation process of nano-ZnO array, characterizes the morphology and structure of the material, and changes and modifies the practical substrate. In this way, the ZnO nanomaterial could apply to a wider range of children's furniture, become more durable, and realize efficient multi-mechanism synergistic sterilization. Tables 1 and 2 list the reagents and instruments/equipment of our experiments.

ZnO has multiple crystal structures. The hydrothermal method of ZnO nano-array includes three primary stages: the preparation of the precursor solution of the seed layer, the preparation of the seed layer, and the generation of the nano-array. For high-temperature hard materials like the metal handles of children's furniture, the pulling method can be adopted to generate a ZnO array on a clean and dry rigid substrate. During the generation, the required crystal ion Zn^{2+} is provided by zinc nitrate hexahydrate, and the required OH^- is supplied by the hydrolysis of hexamethylenetetramine. The specific reactions are described by:



During the reactions of the pulling method, the precursor solution of the seed layer forms an even layer of zinc nitrate hexahydrate liquid on high-temperature hard materials like stainless steel sheet, stainless steel mesh, copper sheet, and aluminum sheet. After four or more times of the above pulling and annealing, a seed layer can be obtained from the substrate. Then, the substrate plate is placed in the growth solution for a certain period, and then flushed, dried, and annealed. The reinforced crystalline samples of the residual organic matter can thereby be obtained. Figure 1 shows the flow of generating ZnO nano-array based on high-temperature hard materials.

The ZnO nano-array can also be obtained through hydrothermal operation on the surface of impregnated fibrous material, such as the wood-based boards of children's furniture. Figure 2 explains the flow for generating ZnO nano-array based on fibrous materials. However, the active substrate of the cellulose, different from other substrates, can be complexed with zinc ions. The complexation strengthens the bond between ZnO and the substrate. The specific reactions are given as follows:

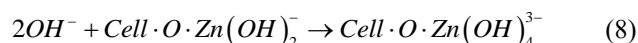


Table 1. Reagents

Name	Specification	Manufacturer
Dihydrate zinc nitrate	Analytically pure	Tianjin Guangfu (China)
Sodium hydroxide	Analytically pure	Tianjin Fengchuan (China)
Isopropanol	Analytically pure	Tianjin Yingcheng (China)
Dihydrate ammonium acetate	Analytically pure	Tianjin Guangfu (China)
Absolute ethyl alcohol	Analytically pure	Tianjin Yingcheng (China)
Hexamethylenetetramine	Analytically pure	Tianjin Fengchuan (China)
Polyethylene glycol octylphenyl ether	Analytically pure	Tianjin Fengchuan (China)
Citric acid	Analytically pure	Tianjin Fengchuan (China)
Triethylamine	Analytically pure	Tianjin Fengchuan (China)
Bacterial cellulose	Food grade	Hainan Yide (China)

Table 2. Instruments and equipment

Name	Manufacturer	Model
Electronic balance	Adam Equipment, Wuhan (China)	PWC124
Thermal field emission scanning electron microscope	OLimp (Japan)	TF2000
High-temperature and high-pressure autoclave	Jiangyin Binjiang (China)	YK-24HDD
Freeze dryer	Ningbo Scientz (China)	SCIENTZ-10N
Electro-heating standing-temperature cultivator	Shanghai Yuejin (China)	HH.B-S
Constant temperature water bath	Gonyi Yuhua (China)	CH1015
High-speed refrigerated centrifuge	Eppendorf (Germany)	3S10R
Water bath oscillator	Haimen Kylin-Bell (China)	QL-901
X-ray diffractometer	Rigaku (Japan)	D/MAX-2500
Cell incubator	Thermal Fisher Scientific (United States)	Therme371
Thermal gravimetric analyzer	Netsch (Germany)	STA4499F3
Universal testing machine	Instron (United States)	Instron3369
Electric furnace	Beijing Zhongxingweiye (China)	DL-1

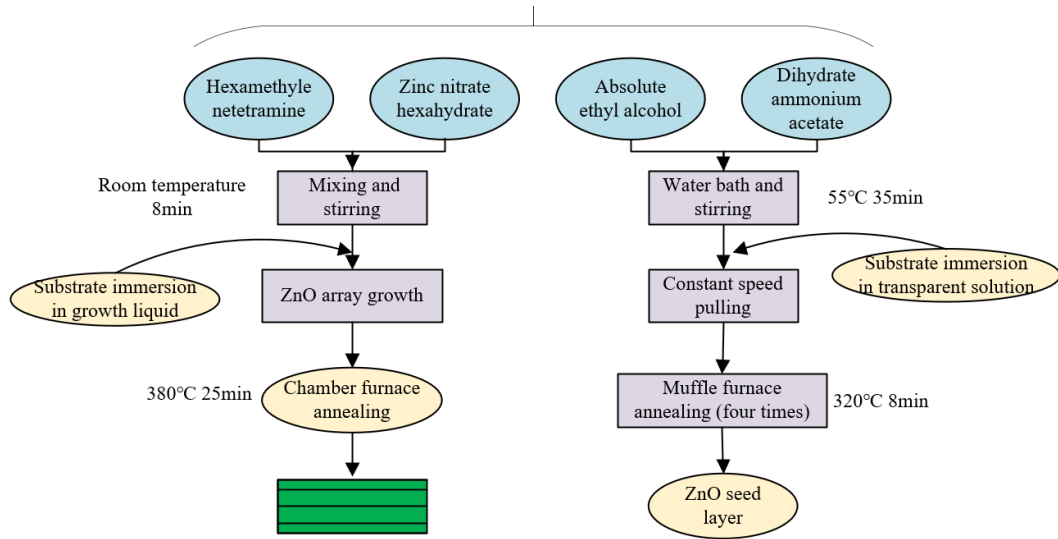
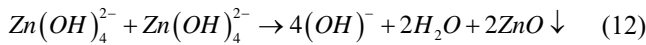
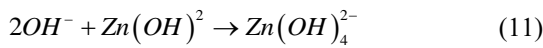
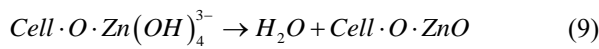


Figure 1. Experimental flow of high-temperature hard materials



The structure of the obtained ZnO crystals was characterized by an X-ray diffractometer at room temperature. Let MG be the mean grain size; ψ be the X-ray wavelength; α be half peak width; $\omega \in [3, 45^\circ]$ be the Bragg diffraction angle. Then, the mean grain size of ZnO can be calculated by:

$$MG = 0.89\psi / (\alpha \cos \omega) \quad (13)$$

Let Q_C be the number-average molecular weight; Q_H be the weight-average molecular weight. Tetrahydropyran and polystyrene were selected as the solvent and the standard sample, respectively. Then, a gel permeation chromatographic analyzer was employed to measure the Q_C and Q_H of the obtained ZnO crystals. The polydispersity index can be calculated by:

$$PDI = \frac{Q_H}{Q_C} \quad (14)$$

Let ε be the mean grain diameter; $\psi_{1/2}$ be the wavelength at the excitation peak or the half-absorption position. Based on the empirical relationship between ε and $\psi_{1/2}$ of ZnO, the particle size of ZnO crystals can be calculated by:

$$\frac{1240}{\psi_{1/2}} = 3.301 + \frac{294.0}{\varepsilon^2} + \frac{1.09}{\varepsilon} \quad (15)$$

Let RQ_{ZnO} be the recovery mass of ZnO nanocrystals. Then, the yield η of ZnO nanomaterials can be calculated by:

$$\eta = \frac{RQ_{ZnO}}{RQ_{(CH_2)_6N_4, 6H_2O} + RQ_{NH_3, H_2O} + RQ_{OH^-} + RQ_{Zn(OH)_2}} \quad (16)$$

2.2 Determination of antibacterial property

The active carboxyl content of cellulose was determined according to the standard TAPPI T237 cm-98. Firstly, a proper amount of cellulose was taken from flexible fibrous materials, treated in hydrochloric acid solution for 2h, and flushed with deionized water. Then, $NaHCO_3$ - $NaCl$ solution was quickly added to the conical flask containing the filtrate. After 1h of reaction, Methyl red indicator was added to the filtrate. Finally, titration was carried out based on hydrochloric acid solution. Let E and F be the hydrochloric acid solution used for titrating the filtrate, and for titrating the $NaHCO_3$ - $NaCl$ solution, respectively; G be the mass of water in the wet slurry cake obtained through the flushing by deionized water; P be the actual concentration of the hydrochloric acid solution; Z be the absolute dry mass of the cellulose sample. Then, the active carboxyl content of cellulose can be calculated by:

$$CAS = \{F - [E + (E \times G / 50)]\} \times P \times (200 / Z) \quad (17)$$

The nitrogen content in and on the zinc acetate solution film were measured by an elemental analyzer. Since ZnO nanomaterials contain no nitrogen, the nitrogen must come from the chitosan of cellulose. Let W and D be the mass of the

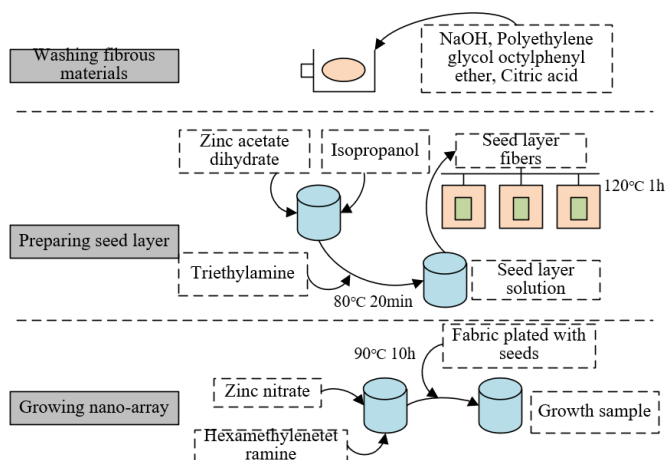


Figure 2. Experimental flow of fibrous materials

zinc acetate solution film before and after flushing, drying, and annealing, respectively. Then, the mass percentage of chitosan on the surface of zinc acetate solution film can be calculated by:

$$CS\% = D/W \times 100\% \quad (18)$$

Next, *Botrytis cinerea*, *Escherichia coli*, and *Staphylococcus aureus* of cell density $1 \times 10^6/\text{mL}$ were inoculated to the crystallized cellulose substrate. On the 1st and 3rd of curing, cell counting was performed with a Cell Counting Kit-8 (CCK-8). Let EGAV and NGAV be the absorbance value of the experimental group, and the absorbance value of the negative group, respectively. Then, the relative cell proliferation rate can be calculated by:

$$RCPR = EGAV / NGAV \times 100\% \quad (19)$$

The diffusion and growth scope of different colonies on each substrate was measured by a vernier caliper. Let GR_O be the mycelial growth range of the reference substrate, and GR_F be that of the substrate containing the ZnO nano-array. Then, the bacteriostasis rate η_{IR} of ZnO nano-array on each colony can be calculated by:

$$\eta_{IR} = \frac{GR_O - GR_F}{GR_O} \times 100\% \quad (20)$$

3. PREPARATION AND ANTIBACTERIAL PROPERTIES OF MODIFIED ZNO NANOMATERIALS

3.1 Preparation and characterization

The dopamine polymer with functional group like primary amine and indole is strongly adhesive and universally applicable. It can deposit on polymers, hard materials, and flexible fibrous materials. If a flexible fibrous material is pre-deposited with polydopamine, the ZnO nanocrystals will concentrate on the cellulose more apparently.

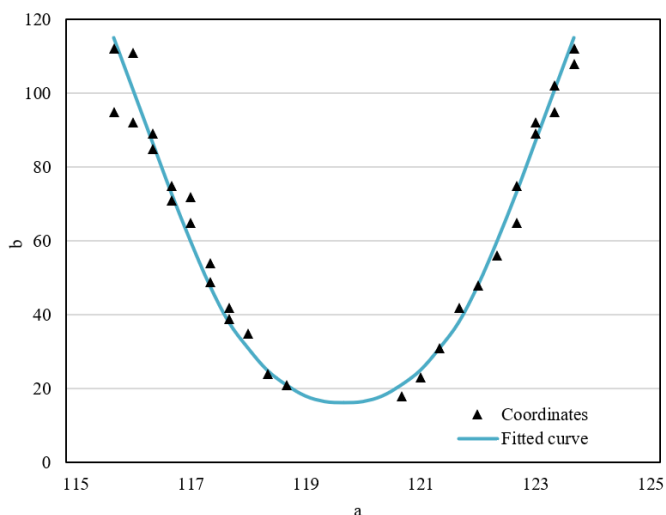


Figure 3. The curve fitted by GaussAMP function

To further determine the relative content of ZnO nanocrystals produced before and after the pre-deposition of

polydopamine particles, this paper carries out a mathematical statistical analysis on ZnO nanocrystals based on image processing techniques. Firstly, Photoshop was adopted to uniformly take several pixels from the ZnO nano-array. Then, the coordinates of each pixel were imported to the function plotting tool Origin 8.5 to draw scatterplots. Finally, each pixel was fitted. The GaussAMP function is employed here:

$$b = b_0 + \delta e^{-\frac{(a-a_0)^2}{2q^2}} \quad (21)$$

The curve fitted by GaussAMP function is shown in Figure 3, where $a \in (-2.2, 2.2)$; b_0 , δ , and $2q^2$ equal -274562, 336452, and 57425, respectively.

Under room temperature, the difference between the two crystal faces before and after the pre-deposition of polydopamine particles can be obtained using ZnO nanocrystal parameters. The difference was characterized by the idea of calculus. Let T and T' be the number of ZnO nanocrystals before and after the pre-deposition of polydopamine particles, respectively; u and e be the total length and width of the exposed crystal surface, respectively. Then, the ratio of the exposed crystals before and after the pre-deposition of polydopamine particles can be calculated by:

$$S = \frac{\sum T^2 u e}{\sum T'^2 u e} \quad (22)$$

3.2 Determination of antibacterial property

Concerning the antibacterial activity of nano-zinc oxide materials in darkness, this paper only considers the final products H₂O₂ and O₂⁻.

Following the KI oxidation-reduction titration, the H₂O₂ produced from the ZnO suspension was determined by measuring the absorbance with a visible spectrophotometer. The measurement was conducted in a completely dark environment. Let XG₄₅₀ be the absorbance value at 450 nm; v be the H₂O₂ content of the solution. Then, the linear regression equation for the standard curve between the H₂O₂ content and absorbance can be fitted as:

$$XG_{450} = 0.132v - 0.0065 \quad (23)$$

Let Vu and Vq be the H₂O₂ contents in u bottles and q bottles of sample solution, respectively; SO be the sampling volume. Then, the yield of the active substance H₂O₂ in the suspension can be calculated by:

$$v = \frac{9(V_u - V_q)(XG_{450} + 0.0065)}{0.6 \times 0.132 \times SO} \quad (24)$$

The O₂⁻ content was estimated by nitro blue tetrazolium. Let XG₂₉₀ be the absorbance value at 290 nm; v' be the O₂⁻ content in the solution. Then, the linear regression equation for the standard curve between the nitro blue tetrazolium content and absorbance can be fitted as:

$$XG_{290} = 0.0421v' + 0.01448 \quad (25)$$

Let Vu' and Vq' be the O₂⁻ contents in u bottles and q bottles of sample solution, respectively; SO' be the sampling volume.

Then, the yield of the active substance O_2^- in the suspension can be calculated by:

$$v' = \frac{9(V'_U - V'_Q)(XG_{290} + 0.0077)}{0.45 \times 0.174 \times SO'} \quad (26)$$

Finally, the antibacterial activity of the prepared ZnO nanoparticles was verified in a dark environment, using three common type strains of the cell density 1×10^6 /mL: Botrytis cinerea, Escherichia coli, and Staphylococcus aureus.

3.3 Thermogravimetric analysis

Let ϕ_{CR} and ϕ_{AP} be the diffraction peak area of the crystalline phase and the amorphous phase, respectively. The crystallinity of ZnO nanocrystals generated before and after the pre-deposition of polydopamine particles can be calculated by

$$CRY = \phi_{CR} / (\phi_{CR} + \phi_{AP}) \times 100\% \quad (27)$$

For the modified antibacterial material based on the prepared ZnO nanocrystals, the mechanical properties can be characterized by breaking strength. Let RI, BS, HD, and KD be the relative strength, breaking strength, thickness, and width of the material, respectively. Then, we have:

$$RI = \frac{BS}{HD \times KD} \quad (28)$$

To further explore the influence of nanoparticle properties over the thermal degradation of modified ZnO nanomaterials, this paper analyzes the modified antibacterial materials based on the thermal degradation reaction kinetics of modified materials. Let PO_s , PO_τ , and PO_e be the weights of the modified material at the start, at time τ , and at the end of the thermal degradation reaction. Then, the weight loss rate of the modified material can be calculated by:

$$\gamma = \frac{PO_s - PO_\tau}{PO_s - PO_e} \quad (29)$$

The thermal degradation rate can be calculated by:

$$\frac{d\gamma}{d\tau} = \Psi g(\gamma) \quad (30)$$

According to the empirical formula of the relationship between chemical reaction rate and temperature, we have:

$$\Psi = SH \cdot e^{-\frac{QB_c}{MG\xi}} \quad (31)$$

where, Ψ is the rate constant; MG is molar gas constant, ξ is thermodynamic temperature; QB_c is apparent activation energy; SH is pre-exponential factor. Let m be the number of reaction stages. The reaction mechanism of the modified material directly determines the function $g(\gamma)$ in formula (30):

$$g(\gamma) = (1 - \gamma)^m \quad (32)$$

Combining formulas (30)-(32):

$$\frac{d\gamma}{d\tau} = SH \cdot e^{-\frac{QB_c}{MG\xi}} (1 - \gamma)^m \quad (33)$$

Taking the log of both sides of formula (33) and finding differentials of $d\gamma/d\tau$, and $1 - \gamma$:

$$\Delta \ln \left(\frac{d\gamma}{d\tau} \right) = -\frac{QB_c}{3.15S} \cdot d(1/\xi) + m \Delta \ln(1 - \gamma) \quad (34)$$

Formula (34) can be converted to a differential form:

$$\Delta \ln \left(\frac{d\gamma}{d\tau} \right) = -\frac{QB_c}{3.15S} \cdot \Delta(1/\xi) + m \Delta \ln(1 - \gamma) \quad (35)$$

Dividing both sides of formula (35) by $\ln(1 - \gamma)$:

$$\frac{\Delta \ln(d\gamma/d\tau)}{\Delta \ln(1 - \gamma)} = -\frac{QB_c}{3.15S} \cdot \frac{\Delta(1/\xi)}{\Delta \ln(1 - \gamma)} + m \quad (36)$$

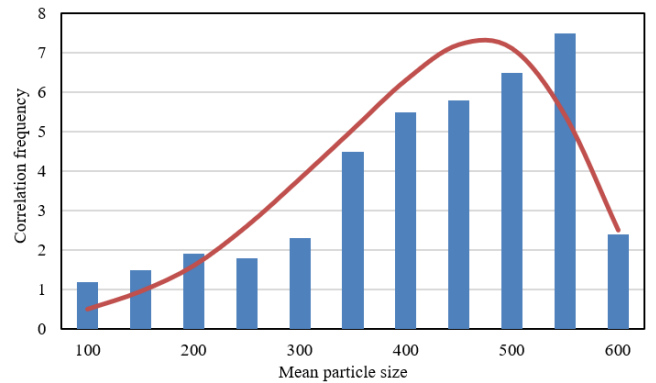
Since $d\gamma/d\tau = (d\gamma/d\xi) \times (d\xi/d\tau)$, we have:

$$\frac{\Delta \ln(d\gamma/d\tau)}{\Delta \ln(1 - \gamma)} = \frac{\Delta \ln(d\gamma/d\xi)}{\Delta \ln(1 - \gamma)} \quad (37)$$

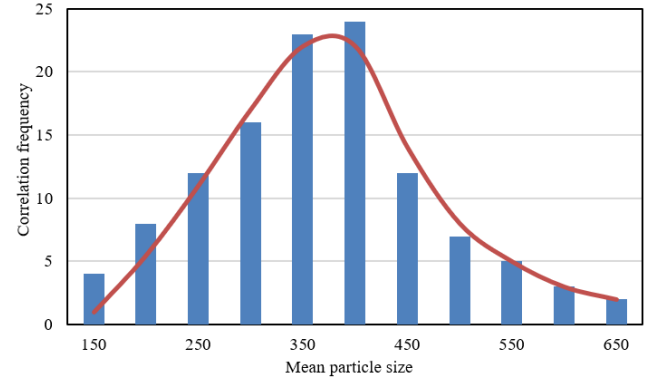
That is:

$$\frac{\Delta \ln(d\gamma/d\xi)}{\Delta \ln(1 - \gamma)} = -\frac{QB_c}{3.15S} \cdot \frac{\Delta(1/\xi)}{\Delta \ln(1 - \gamma)} + m \quad (38)$$

4. EXPERIMENTS AND RESULTS ANALYSIS



(a)



(b)

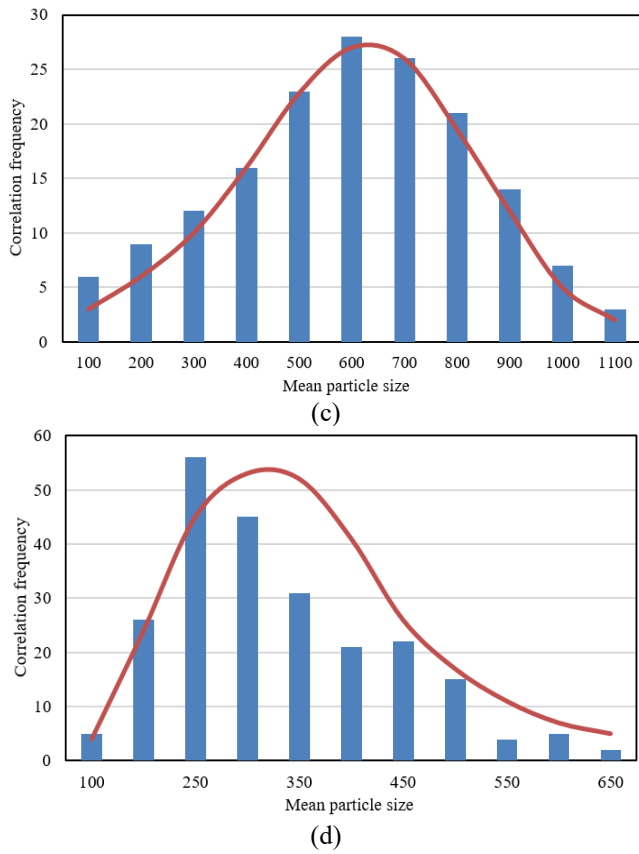


Figure 4. Particle size distribution of ZnO nanocrystals

Figure 4 shows the particle size distribution of the modified ZnO nanocrystals obtained with growth solution of different concentrations: 6mmol/L, 12mmol/L, 24mmol/L, and 30mmol/L. It can be seen that growth solution concentration significantly affected the particle size distribution of the ZnO crystals in the modified material. As the growth solution concentration increased from 6mmol/L to 30mmol/L, the mean particle size of ZnO nanocrystals first increased and then gradually decreased. This means the rising concentration of the growth solution pushes up the zinc ion content, and the number of ZnO crystals. As a result, more active sites appear as zinc ions are absorbed by the cellulose substrate. When the growth solution reaches a certain concentration, the zinc ions outside the cellulose substrate are directly bonded, impeding the crystallization of ZnO on substrate surface. Hence, the number and mean particle size of ZnO crystals both dropped gradually.

Table 3 provides the statistics on the particle size and antibacterial property of ZnO nanocrystals with growth solution of different concentrations. The largest quantity and most antibacterial ZnO were observed at the growth solution concentration of 24mmol/L and the particle size of 432.58nm, followed by 30mmol/L and 395.26nm. The above statistics echo with the antibacterial rates on *Botrytis cinerea*, *Escherichia coli*, and *Staphylococcus aureus*.

Table 4 summarizes the molecular weight and yield of modified material samples at different recovery mass fractions of ZnO nanocrystals. It can be inferred that, with the growth of ZnO mass fraction, the molecular weight of the modified material decreased, that is, the ratio and concentration of the solvent negatively affect the molecular weight of the modified material. In addition, with the increase of the recovery mass fraction of ZnO nanocrystals, the yield of modified material samples decreased. The main reason is that the repeated

flushing with denoised water wash away the impurities in the growth solution, namely, dopamine polymer and citric acid. Hence, the recovery mass fraction of ZnO nanocrystals should be controlled within 3%. Figure 5 gives the XRD images and attenuated total reflection (ATR)- Fourier-transform infrared spectroscopy (FTIR) images of different modified material samples, which further validate the above conclusions.

Table 3. Particle size and antibacterial property of ZnO nanocrystals with growth solution of different concentrations

Growth solution concentration	6	12	24	30
Mean particle size	340.85	432.58	578.29	395.26
Probability of effective antibacterial ZnO	5.28E-06	1.06E-02	0.075	6.02E-01
Number of effective antibacterial ZnO	5.28E-06	0.00445	0.69258	0.04685

Table 4. Molecular weight and yield of different samples

Sample number	1	2	3	4	5	6
Q_c	24562	46253	35284	32648	32477	30254
Q_H	36859	81549	66348	56984	56481	46251
PDI	1.47	1.78	1.82	1.76	1.72	1.55
η	53.4	95.4	93.4	82.4	53.4	28.7

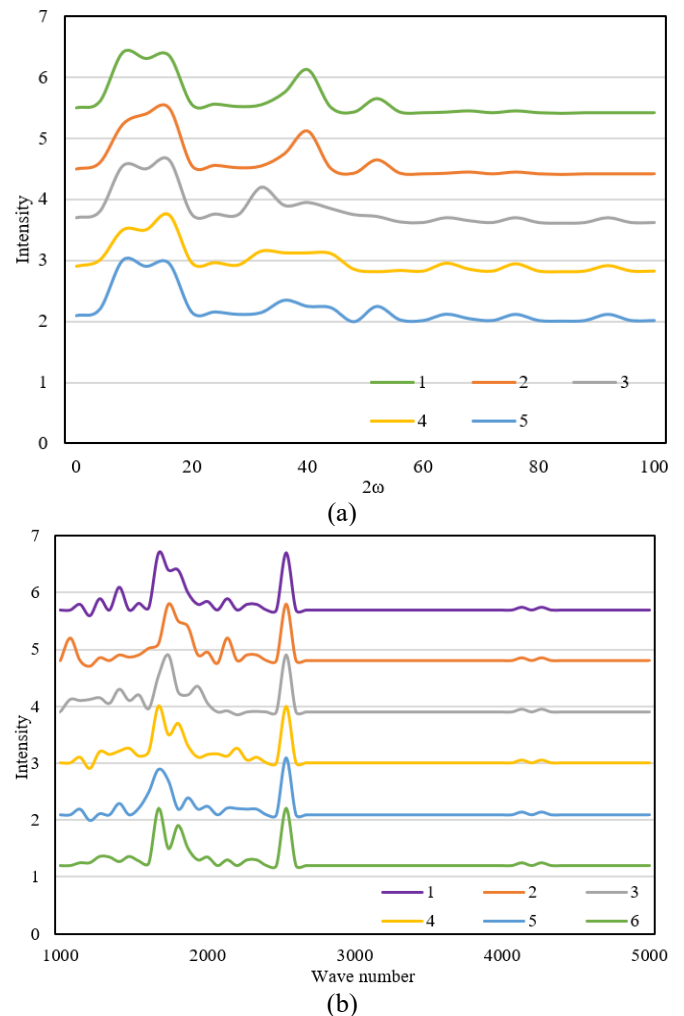


Figure 5. XRD and ATR-FTIR images of different modified material samples

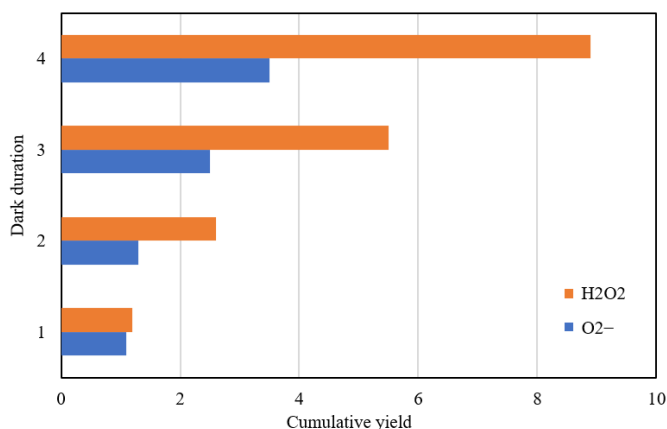


Figure 6. Cumulative yield of final products H₂O₂ and O₂⁻ under dark conditions

Table 5. The residual mass of the modified material with different mass losses at the temperature of 650°C

Sample	No polydopamine	3%	5%	7%
Mass 6%	413.56	375.29	370.11	366.25
loss 12%	400.23	362.54	356.42	362.15
650°C (%)	0	2.14	4.74	5.59

Three common type strains, namely, *Botrytis cinerea*, *Escherichia coli*, and *Staphylococcus aureus*, were selected to verify the antibacterial activity of the prepared ZnO nanomaterial under dark conditions. Figure 6 shows the cumulative yield of final products H₂O₂ and O₂⁻ under dark conditions. It can be observed that the prepared ZnO nanomaterial can suppress nearly 99.9% of the bacteria. The minimal inhibitory concentration was 200, 250, and 300 mg/L against the three common type strains. The performance is better than any ZnO nanostructure material available in the market. Table 5 shows the residual mass of the modified material with different mass losses at the temperature of 650°C. The results indicate that the pre-deposition of polydopamine improves the crystallinity of the modified material, and promotes the growth of ZnO nanocrystals. At 650°C, the residual mass of the modified material was 2.14g, 4.74g, and 5.59g, respectively, which is not very different from the actual dose.

The antibacterial activity of the prepared material, before and after the pre-deposition of polydopamine, against the three common type strains can be measured by the minimal

inhibitory concentration. Figure 7 and Table 6 report the variation of minimal inhibitory concentration before and after pre-deposition of polydopamine. After the pre-deposition of polydopamine, the modified ZnO nanomaterial became stronger in antibacterial activity. Compared with the other two type strains, *Staphylococcus aureus* has a high resistance to modified ZnO nanomaterial. The main reason is that the carotenoid in *Staphylococcus aureus* enhances the resistance to ZnO oxidation stress to a certain extent.

To verify the safety of applying the prepared modified material in children's furniture, this paper explores the toxicity of the material before and after pre-deposition of polydopamine to HUVECs by the CCK-8 method. The toxicity test results (Figure 8) show that the in vitro toxicity of the modified ZnO nanomaterial to HUVECs is dose-dependent. At a low concentration, the modified material promotes cell growth. The cytotoxicity of the modified ZnO nanomaterial hinges on the grain size, shape, and surface modification of its crystals. A high dose of the material greatly impacts the mitochondrial injury and apoptosis. Therefore, the modified ZnO nanomaterial should only be applied to children's furniture in small quantities.

5. CONCLUSIONS

This paper discusses the preparation of a ZnO nanomaterial for children's furniture, and the research and development of antibacterial property. Based on the strengths and defects of ZnO nanomaterial, the authors specified the principle and flow of preparing Zinc nano-array for high-temperature hard materials, and wooden plates, respectively, and analyzed the antibacterial mechanism and antibacterial performance of the zinc nano-array. Then, the enrichment of ZnO nanocrystals on cellulose was improved by pre-depositing polydopamine particles. Through experiments, the particle size distribution of ZnO nanocrystals was analyzed; the particle size and antibacterial effect of ZnO crystals were determined at different concentrations of the growth solution; the XRD and ATR-FTIR images were plotted for different modified material samples; the cumulative yield of the final products, namely, H₂O₂ and O₂⁻, were counted under dark conditions; the variation of minimal inhibitory concentration was plotted before and after pre-deposition of polydopamine. The experimental results show that the prepared modified material can achieve a good antibacterial performance.

Table 6. Minimal inhibitory concentrations before and after pre-deposition of polydopamine

Strains		<i>Escherichia coli</i>		<i>Staphylococcus aureus</i>		<i>Botrytis cinerea</i>	
		Before	After	Before	After	Before	After
ZnO suspension concentration (mg/L)	10	+	+	+	+	+	+
	20	+	-	+	+	+	+
	30	+	-	+	+	+	-
	40	-	+	+	+	+	-
	50	-	-	+	-	+	+
	60	+	+	+	+	+	+
	70	+	-	-	-	+	+
	80	+	-	+	+	+	-
	90	+	-	+	-	-	-
	100	+	-	+	+	+	-
	Positive reference	+	+	+	+	+	+
	Negative reference	-	-	-	-	-	-

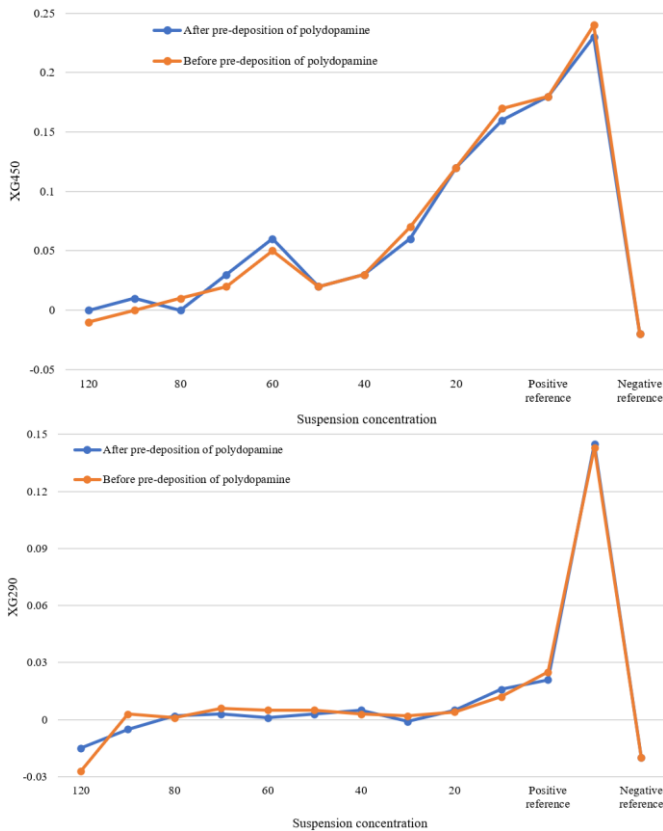


Figure 7. The variation of minimal inhibitory concentration before and after pre-deposition of polydopamine

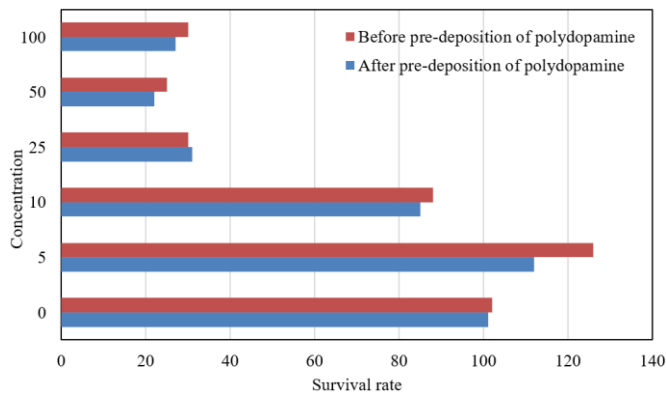


Figure 8. Toxicity test results of modified material on human umbilical vein endothelial cells (HUVECs)

REFERENCES

[1] Christian, Y., Sahroni, T.R. (2020). Green productivity methodology for furniture industry. *IOP Conference Series: Earth and Environmental Science*, 426: 012159. <https://doi.org/10.1088/1755-1315/426/1/012159>

[2] Xu, X., Hua, Y., Wang, S., Xu, G. (2020). Determinants of consumer's intention to purchase authentic green furniture. *Resources, Conservation and Recycling*, 156: 104721. <https://doi.org/10.1016/j.resconrec.2020.104721>

[3] Xu, X., Wang, S., Yu, Y. (2020). Consumer's intention to purchase green furniture: Do health consciousness and environmental awareness matter? *Science of the Total Environment*, 704: 135275. <https://doi.org/10.1016/j.scitotenv.2019.135275>

[4] Zhang, X. (2013). Furniture design based on green ecological environment. In *Informatics and Management Science II*, pp. 283-289. https://doi.org/10.1007/978-1-4471-4811-1_38

[5] Scheithauer, U., Schwarzer, E., Tscharnke, F., Schmidt, T., Jegust, S., Richter, H.J., Moritz, T., Michaelis, A. (2015). New lightweight kiln furniture made by combination of ceramic green tapes and extrudates. *Interceram-International Ceramic Review*, 64(4): 204-208. <https://doi.org/10.1007/BF03401124>

[6] Dotson, S. (2015). Green furniture: An assesment of furniture society member work. *Journal of Green Building*, 10(3): 47-66. <https://doi.org/10.3992/jgb.10.3.47>

[7] Han, J., Li, J., Jiang, Y., Wang, L. (2021). Application of innovative technology in children furniture design. In *E3S Web of Conferences*, 236: 04059. <https://doi.org/10.1051/e3sconf/202123604059>

[8] Jiang, L., Cheung, V., Westland, S., Rhodes, P.A., Shen, L., Xu, L. (2020). The impact of color preference on adolescent children's choice of furniture. *Color Research & Application*, 45(4): 754-767. <https://doi.org/10.1002/col.22507>

[9] Dai, L., Xu, B. (2019). Research on the furniture design criteria for children's psychological development in home environment. In *International Conference on Human-Computer Interaction*, Orlando, FL, USA, pp. 277-286. https://doi.org/10.1007/978-3-030-23538-3_21

[10] Wan, M., Zhang, Y., Ye, W. (2018). Consumer willingness-to-pay a price premium for eco-friendly children's furniture in Shanghai and Shenzhen, China. *Forest Products Journal*, 68(3): 317-327. <https://doi.org/10.13073/FPJ-D-17-00050>

[11] Deng, T., Sun, W., Zhang, R. (2018). Research on parent-child interaction system of intelligent children's furniture based on application behavior analysis. *International Conference on Intelligent Human Systems Integration*, Dubai, United Arab Emirates, pp. 633-638. https://doi.org/10.1007/978-3-319-73888-8_98

[12] Ekaterinushkina, A.V., Zhdanova, N.S., Mishukovskaya, J.I. (2018). Study of functional features of furniture and equipment in the design of recreation of children's polyclinics. *IOP Conference Series: Materials Science and Engineering*, 463(3): 032028. <https://doi.org/10.1088/1757-899X/463/3/032028>

[13] Andaç, T., Güzel, A. (2017). Attitudes of families with children towards eco-friendly designed furniture: Kayseri sample. *BioResources*, 12(3): 5942-5952. <http://doi.org/10.15376/biores.12.3.5942-5952>

[14] Lu, C.W., Lu, J.M. (2017). Evaluation of the Indonesian National Standard for elementary school furniture based on children's anthropometry. *Applied Ergonomics*, 62: 168-181. <https://doi.org/10.1016/j.apergo.2017.03.004>

[15] Dsingh, A. (2017). Degree of musculoskeletal pain and other discomforts experienced by school children using different type of furniture during class. *International Conference on Research into Design*, Guwahati, India, pp. 893-903. https://doi.org/10.1007/978-981-10-3518-0_77

[16] Wan, M., Toppinen, A. (2016). Effects of perceived product quality and lifestyles of health and sustainability (LOHAS) on consumer price preferences for children's furniture in China. *Journal of Forest Economics*, 22: 52-67. <https://doi.org/10.1016/j.jfe.2015.12.004>

- [17] Yuan, Z.Y., Lei, Y.F., Dong, H., Meng, F.L. (2021) Sensitivity analysis of ZnO nanometer gas sensor based on dynamic temperature modulation. *Journal of Northeastern University (Natural Science)*, 42(4): 469-477. <https://doi.org/10.12068/j.issn.1005-3026.2021.04.003>
- [18] Hermida-Montero, L.A., Paraguay-Delgado, F., Cruz, L. F., Carrillo, D., Mtz-Enriquez, A.I., Pariona, N. (2021). The role of coating and size of ZnO nanoparticles on the antifungal activity against *Raffaella* species. *Materials Letters*, 301: 130314. <https://doi.org/10.1016/j.matlet.2021.130314>
- [19] La, D.D., Nguyen-Tri, P., Le, K.H., Nguyen, P.T., Nguyen, M.D.B., Vo, A.T., Nguyenh, M.T.H., Chang, S.W., Tran, L.D., Chung, W.J., Nguyen, D.D. (2021). Effects of antibacterial ZnO nanoparticles on the performance of a chitosan/gum Arabic edible coating for post-harvest banana preservation. *Progress in Organic Coatings*, 151: 106057. <https://doi.org/10.1016/j.porgcoat.2020.106057>
- [20] Li, C., Wang, C., Li, Z., Cao, Z., Xie, Y., Xue, M., Zhao, J. (2021). Preparation of ZnO nanoparticle/acrylic resin superhydrophobic coating via blending method and its wear resistance and antibacterial properties. *Materials*, 14(14): 3775. <https://doi.org/10.3390/ma14143775>
- [21] Tuong, V.M., Huyen, N.V., Kien, N.T., Dien, N.V. (2019). Durable epoxy@ ZnO coating for improvement of hydrophobicity and color stability of wood. *Polymers*, 11(9): 1388. <https://doi.org/10.3390/polym11091388>
- [22] Pang, S., He, Y., Zhong, R., Guo, Z., He, P., Zhou, C., Xue, B., Wen, X., Li, H. (2019). Multifunctional ZnO/TiO₂ nanoarray composite coating with antibacterial activity, cytocompatibility and piezoelectricity. *Ceramics International*, 45(10): 12663-12671. <https://doi.org/10.1016/j.ceramint.2019.03.076>